Characterization of moyamoya disease molecular subtypes through disulfidptosis-related genes and immune landscape analysis

YANRU WANG[1*], YUTAO SU[1*], JUNZE ZHANG[1,2], ZHENYU ZHOU[1], YUANLI ZHAO[3], SHIHAO HE[1,3,4] and RONG WANG[1,5]

[1]Department of Neurosurgery, Beijing Tiantan Hospital, Capital Medical University, Beijing 100070, P.R. China; [2]Department of Pathology, Stanford University School of Medicine, Stanford, CA 94305, USA; [3]Department of Neurosurgery, Peking Union Medical College Hospital, Peking Union Medical College and Chinese Academy of Medical Sciences, Beijing 100730, P.R. China; [4]Department of Neurosurgery, Stanford University School of Medicine, Stanford, CA 94305, USA; [5]China National Clinical Research Center for Neurological Diseases, Beijing 100070, P.R. China

Received October 20, 2024; Accepted January 30, 2025

DOI: 10.3892/etm.2025.12824

Abstract. Moyamoya disease (MMD), a chronic cerebrovascular disorder, is characterized by progressive stenosis of major intracranial arteries. However, the mechanisms underlying the pathological narrowing have remained largely elusive. Disulfidptosis is a new mode of cell death caused by the vulnerability of the actin cytoskeleton to disulfide stress, and proteomic profiling of MMD has revealed that abnormal proliferation of endothelial cells may be induced by upregulation of focal adhesion-related proteins. However, the role of disulfidptosis in MMD has not yet been reported. The Gene Expression Omnibus database was searched for datasets with a sample size of more than six and four microarray datasets (GSE189993, GSE157628, GSE141024 and GSE141022) were downloaded. Based on the expression profiles of DRGs in each sample, MMD was clustered into three discrete molecular subtypes. Differential expression analysis was performed using the R package 'limma' to analyze the differences in gene expression between MMD and controls. Functional enrichment analysis was used to explore the molecular functions and mechanisms of the differentially expressed DRGs in MMD. Based on the results of differential expression analysis, the intersection among four comparison groups, which included C1 vs. C2, C1 vs. C3, C2 vs. C3, and MMD vs. controls, were taken and four hub genes were selected for further study. In addition, the expression and distribution of 22 types of immune cells in each sample was analyzed. Spearman's correlation analysis was performed to explore the correlation between the hub genes and the proportion of immune cells. MMD-related genes were identified and the relationship between them and hub genes was analyzed. Furthermore, ELISA was performed to verify the expression of the four MMD hub genes. In the present study, a novel molecular classification of MMD based on disulfidptosis gene expression was established and a total of 348 upregulated and 801 downregulated genes were identified in patients with MMD compared with controls. A total of four hub genes (*WDR27*, *OSBPL11*, *MSOM1* and *NEIL2*) were selected as biomarkers for the different subtypes of MMD. The DRG results indicated that disulfidptosis may affect the progression of MMD pathogenesis. Based on this, MMD molecular subtypes were constructed and four hub genes were selected. Immune infiltration analysis indicated a relationship between hub genes and immune dysfunction, which could lead to abnormal migration and proliferation of endothelial cells in MMD. The results of the gene set enrichment analysis and gene set variation analysis correlated with the results of immune dysfunction. Differential analysis of MMD-related genes revealed that *MEG3*, *NCL*, *NFIB* and others were significantly differentially expressed in patients with MMD compared to controls. *NEIL2* showed a significant positive correlation with *MEG3* expression (Pearson's r=0.4), whereas *WDR27* showed a significant negative correlation with *MEG3* expression (Pearson's r=0.415). Correlation analysis showed that the four hub genes were significantly associated with endothelial migration- and proliferation-related genes. ELISA revealed that four hub genes (*WDR27*, *OSBPL11*, *MSOM1* and *NEIL2*) were significantly decreased in MMD compared to healthy controls, which correlated with the results of the

Correspondence to: Dr Shihao He, Department of Neurosurgery, Peking Union Medical College Hospital, Peking Union Medical College and Chinese Academy of Medical Sciences, 1 Shuaifuyuan, Dongcheng, Beijing 100730, P.R. China
E-mail: heshihaoo@outlook.com

Professor Rong Wang, Department of Neurosurgery, Beijing Tiantan Hospital, Capital Medical University, 119, South 4th Ring West Road, Beijing 100070, P.R. China
E-mail: ronger090614@126.com

*Contributed equally

Key words: moyamoya disease, disulfidptosis, bioinformatics, molecular subtype, immune infiltration, biomarkers

present bioinformatic analyses. In conclusion, disulfidptosis may be involved in the pathogenesis of MMD. Immune infiltration analysis demonstrated immune dysregulation among different disulfidptosis subtypes, which may lead to the migration and proliferation of endothelial cells. The present study was the first to explore the correlation between MMD pathogenesis and disulfidptosis, providing novel insights and identifying potential subtype classifications and biomarkers for the diagnosis of MMD.

Introduction

Moyamoya disease (MMD), first described by Suzuki and Takaku (1) in 1969, is a chronic cerebrovascular disease presenting with an abnormal vessel net resembling a 'puff of smoke' at the skull base on angiography. MMD presents with progressive occlusion of the terminal portion of the internal carotid artery and circle of Willis, which is recognized as a major cause of ischemic and hemorrhagic strokes (2). The etiology and pathogenesis of MMD remain to be fully elucidated; however, numerous studies have demonstrated that genetic factors, immune function and hemodynamic factors may be responsible for disease progression (3-5). An autopsy case report demonstrated that marked narrowing of cerebral arteries and fibrocellular intimal thickening, which was composed of smooth muscle cells, existed in a patient with MMD (6). The proteomic profiling of MMD has revealed that abnormal endothelial cell proliferation may be induced by the upregulation of focal adhesion-related proteins (7). However, there are still no efficient and sensitive biomarkers for MMD diagnosis or treatment and there is an urgent need to elucidate molecular mechanisms underlying MMD initiation and progression to identify therapeutic and diagnostic targets.

Disulfidptosis is a newly identified form of cell death caused by the vulnerability of the actin cytoskeleton to disulfide stress induced by the collapse of aberrant disulfide bonds in actin cytoskeleton proteins and F-actin (8). The amino acid transporter protein solute carrier family 7 member 11 helps transport cystine to cancer cells, which promotes tumor growth. Cystine, a toxic disulfide, accumulates in tumor cells and triggers disulfidptosis when cells lack glucose, and NADPH production decreases, which can convert cystine into non-toxic molecules (8,9). *RNF213* was identified as a susceptibility gene for MMD. *RNF213* knockdown in vascular smooth muscle cells led to alteration in cytoskeletal organization and contractility (10). The protein profiling of MMD also revealed upregulated cytoskeletal proteins (7). Furthermore, exosomal micro (mi)RNA profiling revealed significant differences in the expression of miRNAs involved in vascular cytoskeleton reconstruction in MMD (11). The dysregulation of the cytoskeleton in MMD may be involved in abnormal disulfidptosis, which is caused by the vulnerability of the actin cytoskeleton, and aberrant disulfidptosis may be involved in abnormal cell proliferation during the pathogenesis of MMD.

The present study aimed to identify possible pathogenic mechanisms of MMD, and comprehensive bioinformatics analyses were used to explore disulfidptosis-related genes (DRGs) in MMD using the Gene Expression Omnibus (GEO) database. The expression profiles of DRGs in MMD were analyzed, and consistency clustering analysis was performed to construct subclusters of MMD. Functional enrichment analysis was also performed for different molecular subtypes of MMD. Furthermore, hub genes with intersecting gene sets of differential DRGs were identified among different molecular subtypes and between patients with MMD and controls. Immune infiltration was further explored and its correlation with hub genes was assessed. Analyses of signaling pathways and transcription regulation were used to explore the functions and regulatory mechanisms of hub genes in MMD. The whole study provides comprehensive analyses of disulfidptosis in MMD and new insights into the molecular pathological mechanisms of MMD.

Materials and methods

Data processing. This study was approved by the Ethics Committee of Beijing Tiantan Hospital (Beijing, China; approval no. KY-2023-2024-02). To identify relevant gene expression datasets, a comprehensive search was performed using the keyword 'moyamoya disease' in the GEO database (https://www.ncbi.nlm.nih.gov/geo/), selecting studies with *Homo sapiens* as the species. Datasets with a sample size greater than six were included to ensure sufficient statistical power and four microarray datasets (GSE189993, GSE157628, GSE141024 and GSE141022) were obtained (12,13). For each dataset, gene expression files were downloaded and the same platform, GPL16699, was used for data analysis. These datasets were composed of gene expression profiles from middle cerebral artery (MCA) samples. Specifically, the matrix data file of GSE189993 included the gene expression data of 32 participants (21 patients with MMD and 11 healthy controls), and GSE157628 contained the gene expression data of 20 participants (11 patients with MMD and 9 healthy controls). The matrix data file GSE141024 was obtained from eight participants (four patients with MMD and four healthy controls), and GSE141022 included the expression profiles from eight participants (four patients with MMD and four healthy controls). Detailed sample information for each dataset, including the number of patients with MMD and control subjects, is presented in Table SI. The R package SVA was used to correct the microarrays and display the status of the batches before and after correction using principal component analysis.

Consistency clustering analysis of DRGs. The DRG gene set was obtained from a study by Liu *et al* (8). Based on the expression profiles of the DRGs for each sample, the data were clustered into discrete molecular clusters, and 90% of the total samples were clustered using 300 iterations (8). A consensus cumulative distribution function (CDF) curve was constructed and a consensus matrix heatmap analysis was performed to choose the best cluster number κ (κ=3) to distinguish different molecular subtypes of MMD (C1, C2 and C3) for further analyses.

Differential expression analysis. Differential expression analysis was performed using the R package 'limma' with R (version 4.2.2) to analyze the differences in gene expression between subjects with MMD and controls with the Mann-Whitney U-test. Differences in the expression profiles

were also identified among the molecular subtypes of MMD with the Kruskal-Wallis H-test. Differentially expressed genes were selected using the conditions of P<0.05, |$\log_2$fold change (FC)|>1. Heatmaps were drawn to show the gene expression differences using the R package 'ggplot2' with R (version 4.2.2). Differential DRGs were obtained and further analyzed using Spearman correlation analysis in patients with MMD and controls.

Functional enrichment analysis. Functional enrichment analysis was used to explore the molecular functions and mechanisms of the differentially expressed DRGs in MMD. Gene ontology (GO) enrichment analysis and Kyoto Encyclopedia of Genes and Genomes (KEGG) pathway enrichment analysis were performed using the R package 'clusterProfiler' with R (version 4.2.2). P- and q-values of less than 0.05 were considered to indicate statistical significance.

Identification of hub genes in MMD. Based on the results of the differential expression analysis that selected genes with a P-value <0.05 and |log2FC|>1, the intersecting differentially expressed genes were selected from four comparison groups, which included C1 vs. C2, C1 vs. C3, C2 vs. C3, and MMD vs. controls, which included 29 differentially expressed genes. Using the intersecting gene sets, they were ranked according to the average functional similarity correlation using Friend analysis and the top five genes with the highest correlation were selected as candidate hub genes. Furthermore, intergroup differential expression analysis was performed using the Kruskal-Wallis H-test with candidate hub genes among C1, C2, C3 and the controls, which were used to select significantly differentially expressed genes among these groups as hub genes for further study.

Immune infiltration analysis. Immune cell profiling was performed using the CIBERSORT algorithm, a robust method for evaluating immune cell composition in tissue samples. The CIBERSORT tool is based on a reference set of 547 gene markers representing 22 distinct human immune cell types (14). A differential analysis of immune cell expression was conducted to investigate the immune characteristics across different molecular MMD subtypes with the Kruskal-Wallis H-test. This analysis revealed significant differences in immune cell infiltration between patients with MMD and healthy controls with the Mann-Whitney U-test. Additionally, Spearman correlation analysis was performed to explore the potential associations between the expression of hub genes and the relative proportions of specific immune cell types.

Gene set enrichment analyses (GSEA) of hub genes. The differences in the signaling pathways of the hub genes between the high- and low-expression groups were further analyzed using GSEA. The annotated gene set of version 7.0 was obtained from the MsigDB database (https://www.gsea-msigdb.org/gsea/msigdb). Significantly enriched gene sets (with an adjusted P<0.05) were sorted based on consistency scores.

Gene set variation analysis (GSVA). GSVA, a nonparametric and unsupervised method, is used for evaluating the enrichment of transcriptome gene sets. Gene sets were downloaded from the molecular signature database and the GSVA algorithm was used to comprehensively score each gene set and evaluate the differential biological functions of the hub genes in different samples.

Transcription regulation analysis. The prediction of transcription factors was performed with hub genes using the R package 'RcisTarget' with R (version 4.2.2). All calculations were based on motifs, and the normalized enrichment scores of motifs were scored using motifs from the database and annotation files based on motif similarity and gene sequences. Visualization of a comprehensive transcriptional regulatory network of hub genes for disulfideptosis in MMD was constructed using Cytoscape (version 3.2.1; http://www.cytoscape.org/).

MMD-related gene correlation analysis. MMD-related genes were obtained from the GeneCards database (https://www.genecards.org/) and differential expression analysis was performed using the R package 'limma' with R (version 4.2.2) to compare the expression level of MMD-related genes between disease and control groups with the Mann-Whitney U-test. The relationship between MMD-related genes and hub genes was visualized using a bubble chart and Pearson correlation analysis.

Endothelial migration and proliferation-related gene correlation analysis. Endothelial migration- and proliferation-related genes were obtained from the GeneCards database. Pearson correlation analysis was used to explore the relationship between endothelial migration- and proliferation-related genes and hub genes.

Statistical analysis. All analyses were performed using R (version 4.2.2), and P<0.05 was considered to indicate statistical significance. Comparisons between two groups were performed using the Mann-Whitney U-test and comparisons between three or more groups were performed using the Kruskal-Wallis H-test. All of the correlation analyses used in the study were Pearson correlation analyses.

Participants and sample preparation. A total of three Chinese and Han individuals were enrolled who underwent digital subtraction angiography to check for MMD at the Department of Neurosurgery, Beijing Tiantan Hospital, Capital Medical University (Beijing, China) from July 2021 to December 2022 (15). Detailed consultations and physical examinations of patients with MMD were performed to ensure that they did not have any underlying diseases, such as hypertension, diabetes, hyperlipidemia or hyperthyroidism, or any surgical history, which could have affected the results of this study. Table SII shows the clinical and demographic characteristics of the patients. 3 MMD patients (1 male and 2 females) with an age range of 39 to 51 years were included. And 3 healthy controls (1 male and 2 females) with an age range of 30 to 45 years were included. In addition, three healthy controls (age range, 18-45 years) were recruited with clinical notice in Beijing Tiantan Hospital from July 2021 to December 2022. Written informed consent was obtained from all participants in accordance with the Declaration of Helsinki

and the study protocol was approved by the Ethics Committee of Beijing Tiantan Hospital (Beijing, China; approval no. KY 2020-045-02), which informed the patients that the blood samples would be used in studies of MMD pathogenesis in the future. Blood samples (2 ml) were collected from all patients with MMD and centrifuged at 1,500 x g for 10 min at room temperature, followed by storage at -80˚C for analysis.

Enzyme-linked immunosorbent assay (ELISA). The serum of six participants was obtained after centrifugation and a standard solution was prepared according to the manufacturer's instructions. The Human WDR27 ELISA Kit (cat. no. E16199h; Elabscience; https://www.elabscience.cn/), Human NEIL2 ELISA Kit (cat. no. abx534990), Human MSMO1 ELISA Kit (cat. no. abx385151; both from Abbexa) and Human OSBPL11 ELISA Kit (cat. no. MBS166713; MyBioSource, Inc.) were obtained to perform the assays. Standard, blank and sample wells were used in the ELISA kits. To the standard wells, 100 μl of diluted standard solution was added, while 100 μl of standard diluent buffer was added to the blank wells, and 100 μl of the sample was added to the remaining wells, which were incubated at 37˚C for 1 h. After adding detection reagents A and B to each well by suction and washing, each well was sealed and incubated at 37˚C in the dark for 20 min. Subsequently, 50 μl stop solution was added to each well and the optical density value at 450 nm was measured. Data were analyzed and visualized using GraphPad Prism 9 (version 9.4.0; Dotmatics) and Adobe Illustrator (version 26.3.1; Adobe Systems, Inc.) was used to organize and combine figures. All data are expressed as the mean ± standard deviation. Statistical differences between groups were tested using one-way ANOVA with Tukey's post-hoc test. $P<0.05$ was considered to indicate statistical significance.

Results

Differential expression analysis of DRGs in MMD. The GSE189993, GSE157628, GSE141024 and GSE141022 datasets were downloaded from the GEO database and expression profile data were obtained from 68 participants (40 patients with MMD and 28 controls). The results showed that the batch effect among microarrays was reduced after correction (Fig. 1A). The expression levels of DRGs in samples from MMD and controls were analyzed and the results demonstrated that LRPPRC (FC=-10.4 and P=0.01), NCKAP1 (FC=0.49 and $P=7.33x10^{-5}$) and NDUFS1(FC=0.86 and P=0.04) genes were differentially expressed in MMD compared with the controls (Fig. 1B). A heatmap was drawn to show the expression of DRGs in each sample (Fig. 1C). In addition, a correlation analysis of these genes between the control and MMD samples was conducted, as shown in Fig. 1D.

Functional enrichment analysis of differentially expressed genes. GO and KEGG enrichment analyses were performed and the results are shown as a heatmap in Fig. 1E and F. GO enrichment analysis revealed that the barbed-end actin filament capping process (P=0.005) and myosin V binding (P=0.007) were significantly enriched in differentially expressed genes in MMD (Fig. 1F). KEGG enrichment analysis revealed that DNA replication (P=0.03) and aminoacyl tRNA biosynthesis (P=0.02) pathways were significantly enriched (Fig. 1E).

Molecular subtypes classification based on DRGs in MMD. Consistency clustering was performed and a molecular classification of MMD based on DRG expression levels was constructed. Although the CDF curve showed that $\kappa=2$ was the best choice of molecular subtypes classification, the results showed that the boundaries of the subtypes in the samples were clearer when $\kappa=3$ compared with $\kappa=2$ in Fig. 2A-C, which indicated that MMD should be divided into three clusters.

Identification and expression profiles of hub genes in MMD. To identify hub genes related to MMD and its molecular subtypes, the R package limma was used to perform differential expression analyses of four groups with R (version 4.2.2): C1 vs. C3, C2 vs. C3, C1 vs. C3, and MMD vs. control. The standard for selecting differentially expressed genes was $P<0.05$ and $|logFC|>1$. A total of 2,264 differentially expressed genes were identified for C1 vs. C2, including 1,207 upregulated and 1,057 downregulated genes. A total of 6,547 differentially expressed genes were screened for C2 vs. C3, including 2,976 upregulated and 3,571 downregulated genes. For C1 vs. C3, 5,368 differentially expressed genes were detected, including 2,228 upregulated and 3,140 downregulated genes. Finally, 1,149 differentially expressed genes were screened for MMD vs. controls, including 348 upregulated and 801 downregulated genes. Among the four gene sets, 29 intersecting genes were identified, which are shown as Venn plots (Fig. 2D). Furthermore, the 29 intersecting genes were sorted based on the average functional similarity relationships among proteins and the results showed that *TMEM97*, *WDR27*, *OSBPL11*, *MSMO1* and *NEIL2* were the top five genes (Fig. 2G). Intergroup analysis of these five genes in the control and three MMD molecular subtypes was also performed, and the results showed significant differences among the *WDR27* (P=0.03), *OSBPL11* (P=0.04), *MSMO1* ($P=3.79x10^{-5}$) and *NEIL2* (P=0.003) genes (Fig. 2E and F). Therefore, these four genes were considered hub genes for further analysis.

Immune infiltration analysis and correlation between immune function and hub genes. The distribution of immune cells in each sample is shown in Fig. 3A. An immune cell correlation heatmap is also provided (Fig. 3B). Furthermore, the expression of different immune cells was compared among MMD subtypes. The results showed significant differences in monocyte (P=0.02) and M2 macrophage (P=0.005) counts among the different molecular subtypes (Fig. 3C). The correlation between the hub genes and immune cells in patients with MMD was further explored. *WDR27* was significantly positively correlated with CD4 memory T cells (r=0.40, P=0.01) and memory B cells (r=0.36, P=0.02), but negatively correlated with T cells CD4 naive (r=-0.24, P=0.03) (Fig. 3D). *OSBPL11* was significantly positively correlated with neutrophils (r=0.57 and P=0.0001), but negatively correlated with M0 macrophages (r=-0.47 and P=0.002) and regulatory T cells (Tregs; r=-0.43, P=0.006; Fig. 3E). *MSMO1* was positively correlated with resting dendritic cells (r=0.34, P=0.03), while it was negatively correlated with activated dendritic cells

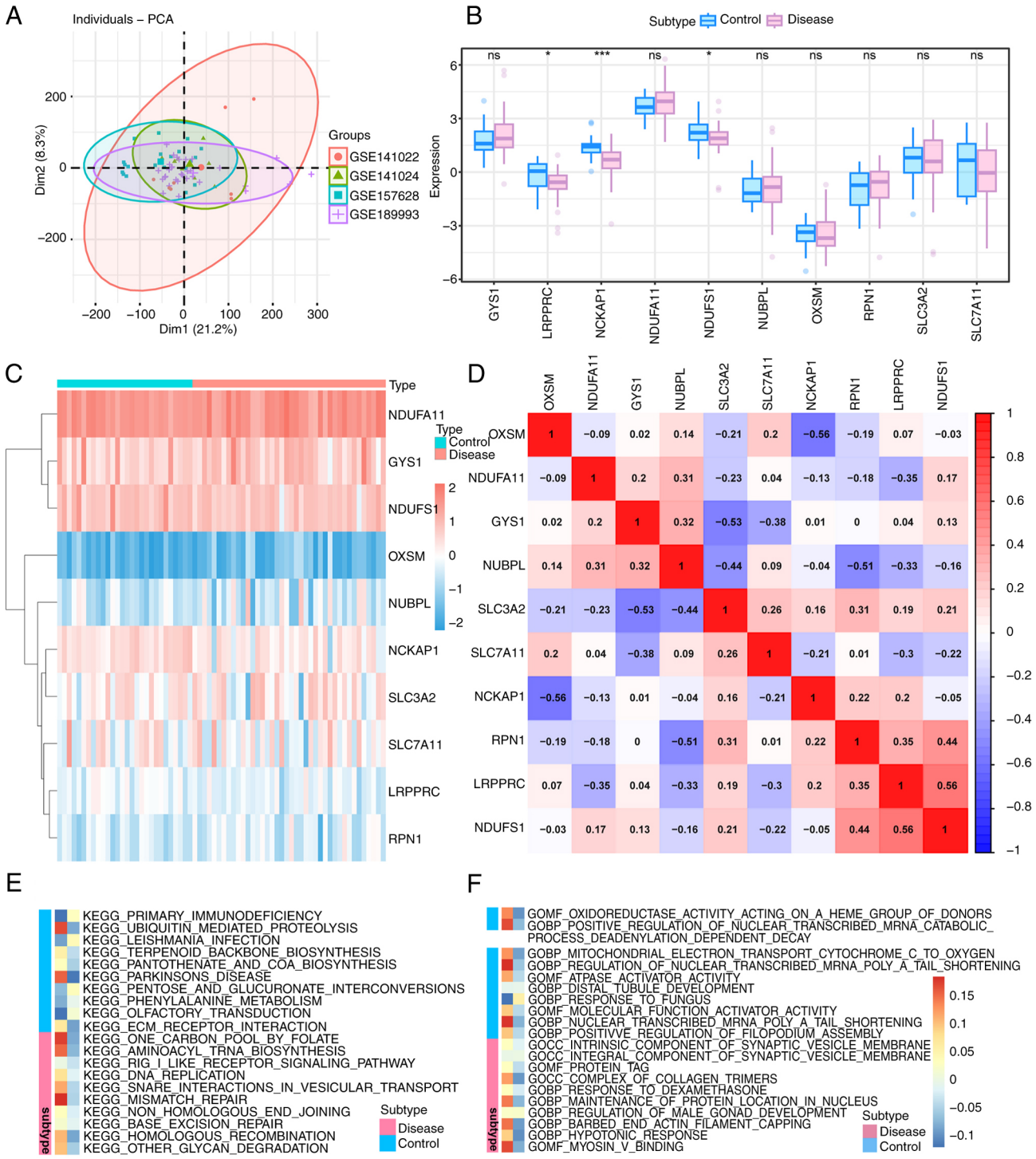

Figure 1. Differential analysis and functional enrichment analysis with gene datasets. (A) PCA plots after correlation. The different colored circles represent different datasets. (B) Box plot of DRGs between MMD group and control group. Blue represents the control group and red represents the MMD group. *P<0.05; ***P<0.001; ns, no significance. (C) Heatmap of DRG expression in MMD and controls. Different colors represent expression levels in each sample. Red indicates upregulation and blue indicates downregulation. (D) Heatmap of correlation analysis among various DRGs in patients with MMD. Red indicates a positive correlation and blue indicates a negative correlation. (E) KEGG enrichment analysis of DRGs in MMD. (F) GO enrichment analysis of DRGs in MMD. The two different columns indicate the different groups, the red one is the disease group and the blue one is the control group. PCA, principal component analysis; GO, gene ontology; BP, Biological Process; CC, Cellular Component; MF, Molecular Function; KEGG, Kyoto Encyclopedia of Genes and Genomes; DRG, disulfide-ptosis-related gene; MMD, moyamoya disease.

(r=-0.32, P=0.04; Fig. 3F). *NEIL2* was significantly positively correlated with neutrophils (r=0.46, P=0.003) and gamma delta T cells (r=0.35, P=0.03), while it was significantly negatively correlated with eosinophils (r=-0.39, P=0.01) and resting natural killer cells (r=-0.32, P=0.04; Fig. 3G).

GSEA and GSVA pathway enrichment analysis. The enriched signaling pathways associated with the four hub genes and the potential molecular mechanisms by which hub genes affect the pathogenesis of MMD were investigated. The GSEA results demonstrated that *NEIL2* was enriched

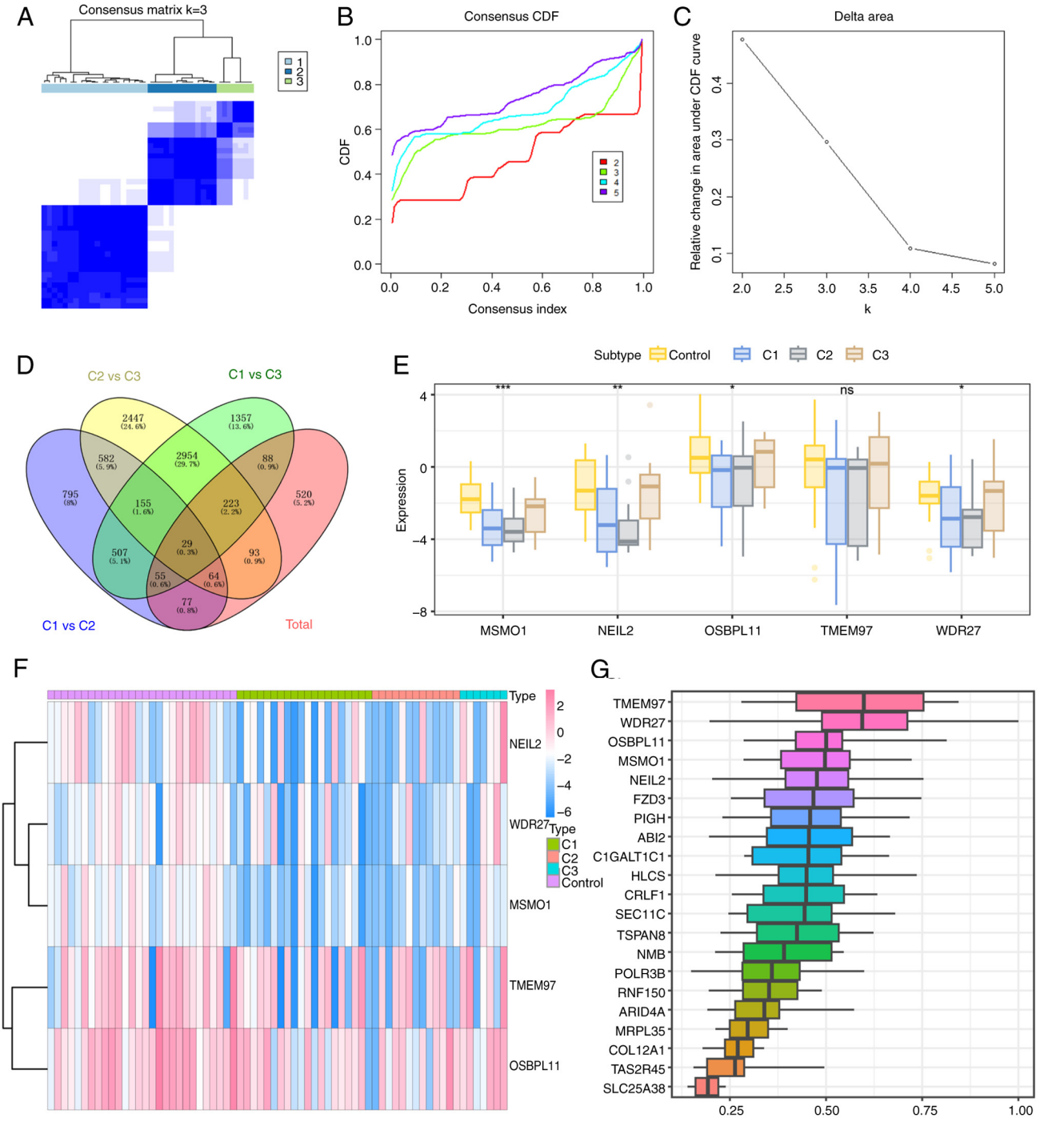

Figure 2. Consistency clustering analysis of disulfide-ptosis-related genes and selection of hub genes in Moya-Moya disease. (A) Consensus matrix map of the consistency clustering analysis when the cluster number is κ=3. (B) Consensus CDF curve of different cluster numbers in the consistency clustering analysis. (C) The delta area curve of different cluster numbers in the consistency clustering analysis. (D) Venn plot of the differentially expressed genes among the four groups. A total of 29 intersecting genes were identified. (E) Box plot of expression levels of differentially expressed candidate hub genes among the four groups. *P<0.05; **P<0.01; ***P<0.001; ns, no significance. (F) Heatmap of the expression levels of candidate hub genes. Red indicates upregulation and blue indicates downregulation. (G) The 29 intersecting genes were sorted based on the average functional similarity relationship among proteins. The x-axis represents the value of similarity measurement from the Friend analysis. CDF, cumulative distribution function.

in pathways, including the chemokine signaling pathway (P=0.0002), ErbB signaling pathway (P=0.006) and phagosome pathway (P=1.43x10^{-5}; Fig. 4A). GSVA indicated that high *NEIL2* expression was enriched in the interferon gamma response (GSVA score=2.94) and apical junction signaling pathways (GSVA score=2.68; Fig. 4B). The pathways enriched by *OSBPL11* included the IL-17 (P=0.002), PPAR (P=0.001) and TNF signaling pathways (P=0.0003; Fig. 4C). GSVA analysis revealed that high expression of *OSBPL11* was enriched in signaling pathways such as interferon gamma response (GSVA score=4.78), apical junction (GSVA score=3.26) and reactive oxygen species pathways (GSVA score=3.35; Fig. 4D). The pathways enriched by *MSMO1* include DNA replication (P=0.005), propanoate metabolism

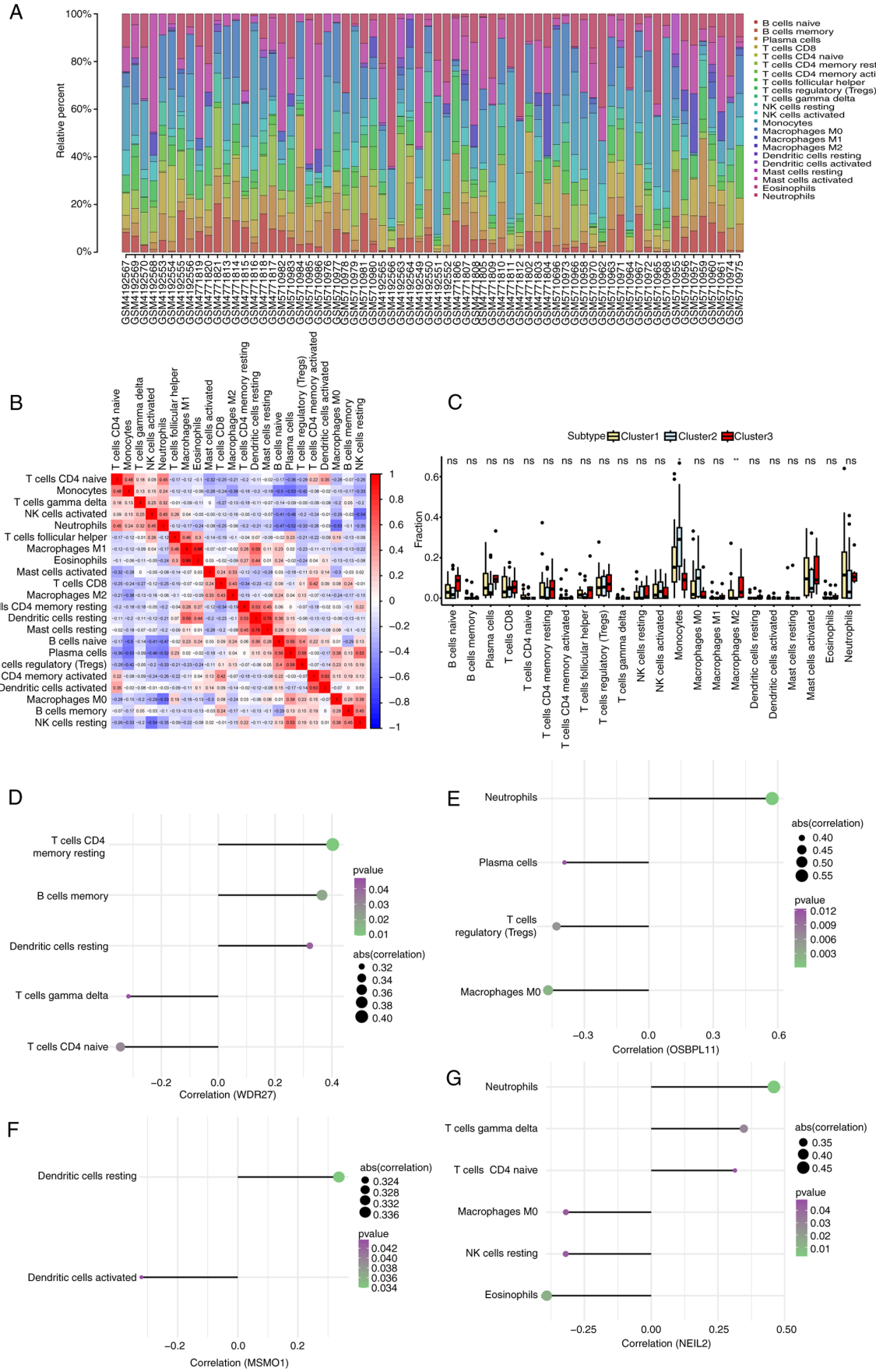

Figure 3. Immune landscape of MMD subtypes compared with controls and the association of immune infiltration and hub genes. (A) Distribution of immune cells in each sample. (B) Heatmap of correlation analysis among different immune infiltration cells in patients with MMD. Red indicates a positive correlation and blue indicates a negative correlation. (C) The expression level of various immune infiltration cells among different MMD molecular subtypes. *P<0.05; **P<0.01; ns, no significance. (D-G) Correlation between 4 hub genes (D) *WDR27*, (E) *OSBPL11*, (F) *MSMO1* and (G) *NEIL2* and immune infiltration cells. MMD, moyamoya disease.

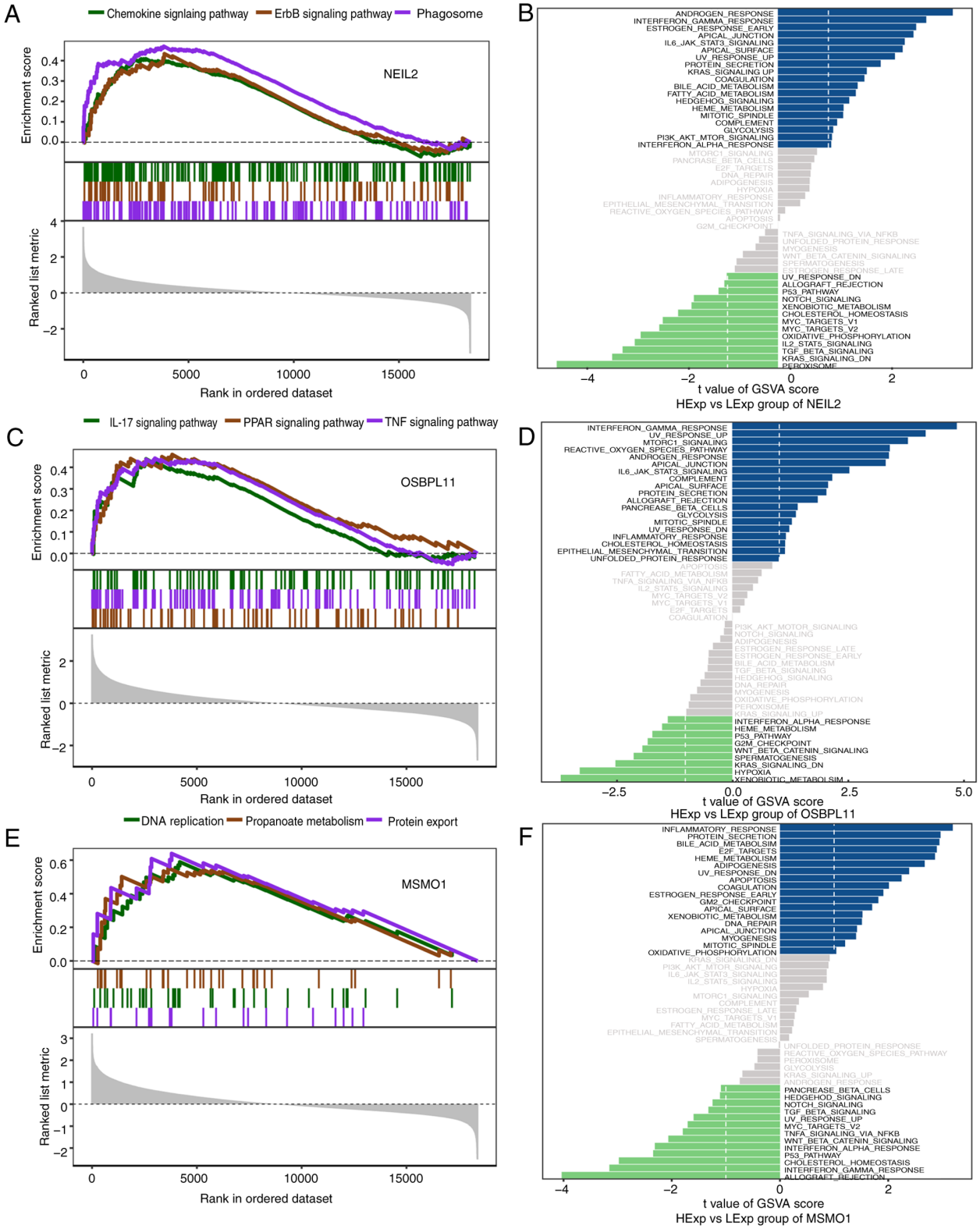

Figure 4. GSVA and GSEA analyses of hub genes. (A) The GSEA shows that *NEIL2* was enriched in pathways including the ErbB signaling pathway and phagosome pathway. (B) The GSVA result for *NEIL2*. High *NEIL2* expression was observed in interferon gamma response and apical junction signaling pathways. (C) The GSEA shows that *OSBPL11* was enriched in the IL-17 and TNF signaling pathways. (D) The GSVA result for *OSBPL11*. High *OSBPL11* expression was observed in interferon gamma response and apical junction pathways. (E) The GSEA shows that *MSMO1* was enriched in DNA replication and protein export pathways. (F) The GSVA result for *MSMO1*. High *MSMO1* expression was observed in inflammatory response and protein secretion. GSEA, gene set enrichment analysis; GSVA, gene set variation analysis.

(P=0.004) and protein export pathways (P=0.002; Fig. 4E) and high *MSMO1* expression was enriched in signaling pathways including inflammatory response (GSVA score=3.19), protein secretion (GSVA score=2.96) and HEME metabolism (GSVA score=2.86; Fig. 4F). *WDR27* enriched pathways included DNA replication (P=0.002), ErbB signaling pathway

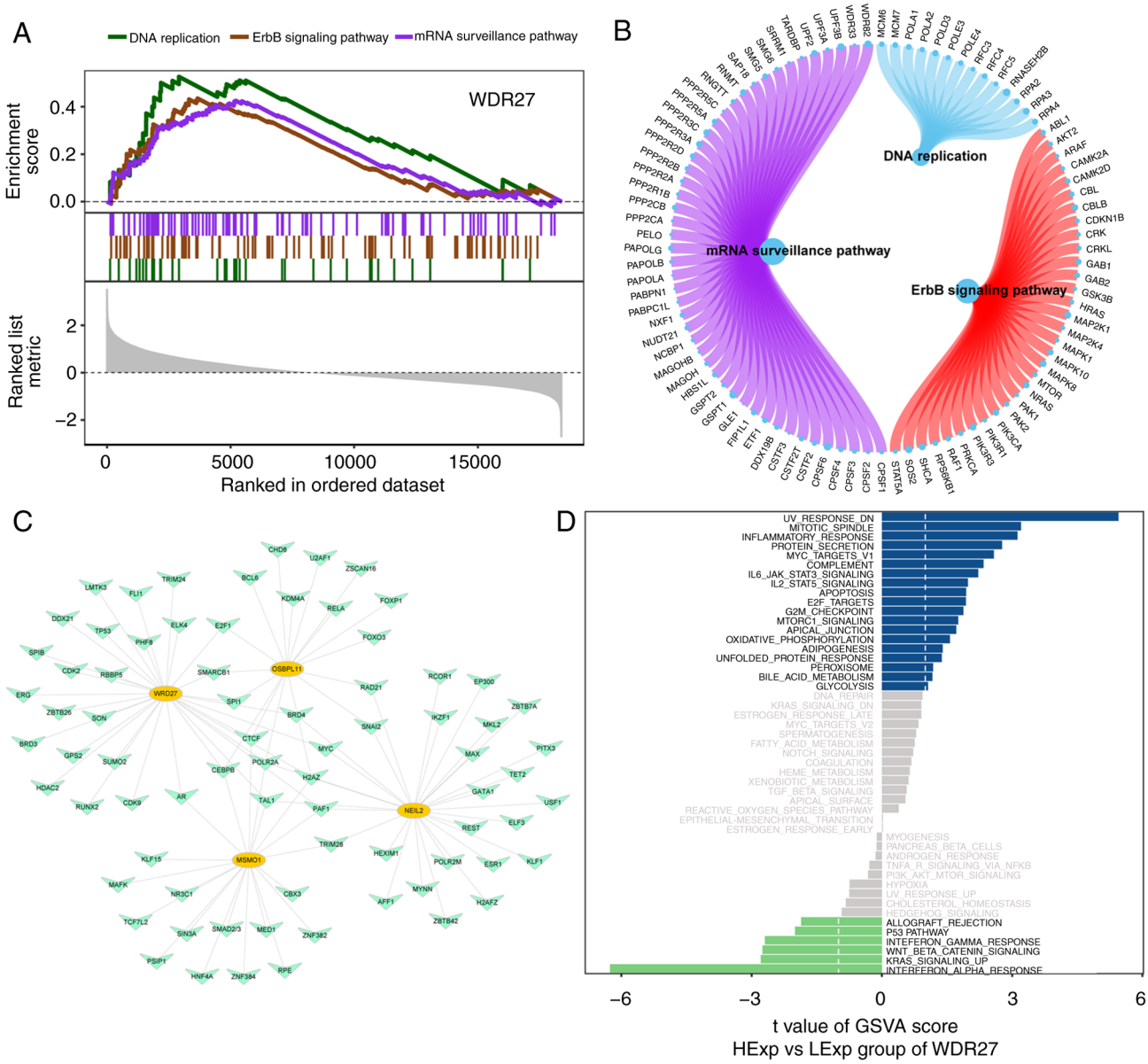

Figure 5. GSVA and GSEA analyses of *WDR27* and transcriptional regulation analysis of hub genes. (A) The GSEA shows that WDR27 was enriched in DNA replication, ErbB signaling pathway and mRNA surveillance pathways. (B) The map of genes related to DNA replication, ErbB signaling pathway and mRNA surveillance pathways. (C) The comprehensive transcriptional regulatory network of hub genes for disulfidptosis in Moya-Moya disease. (D) The GSVA result for *WDR27*. High *WDR27* expression was observed in the inflammatory response and IL6-JAK-STAT3 signaling pathways. GSEA, gene set enrichment analysis; GSVA, gene set variation analysis.

(P=0.002) and mRNA surveillance pathway (P=0.001; Fig. 5A and B). The GSVA results showed that high expression of *WDR27* was enriched in the inflammatory (GSVA score=3.12) and IL6 JAK STAT3 signaling pathways (GSVA score=2.22; Fig. 5D).

Transcriptional regulation of hub gene analysis. Four hub genes were used as gene sets for this analysis to further explore the transcriptional regulatory networks involved in the hub genes. Using the Cistrome DB database, 69 transcription factors were predicted using *MSMO1*, 104 using *NEIL2*, 88 transcription factors were predicted using *OSBPL11* and 107 transcription factors were predicted using *WDR27*. Visualization of a comprehensive transcriptional regulatory network of hub genes for disulfide ptosis in MMD was constructed using Cytoscape (Fig. 5C).

MMD-related genes correlation analysis. Differential analysis of MMD-related genes revealed that *MEG3*, *NCL*, *NFIB* and others were significantly differentially expressed in different molecular groups of MMD, which indicated different gene phenotypes in the molecular classification based on disulfidptosis-related genes (Fig. 6A). The expression levels of hub genes were also significantly correlated with those of various MMD-related genes (Fig. 6B). *NEIL2* showed a significant positive correlation with *MEG3* (Pearson's r=0.4), whereas *WDR27* was negatively correlated with *MEG3* (Pearson's r=0.415).

Endothelial migration and proliferation-related genes correlation analysis. The expression levels of the hub genes were significantly correlated with various endothelial migration-related genes (Table SIII). In particular, *OSBPL11* showed

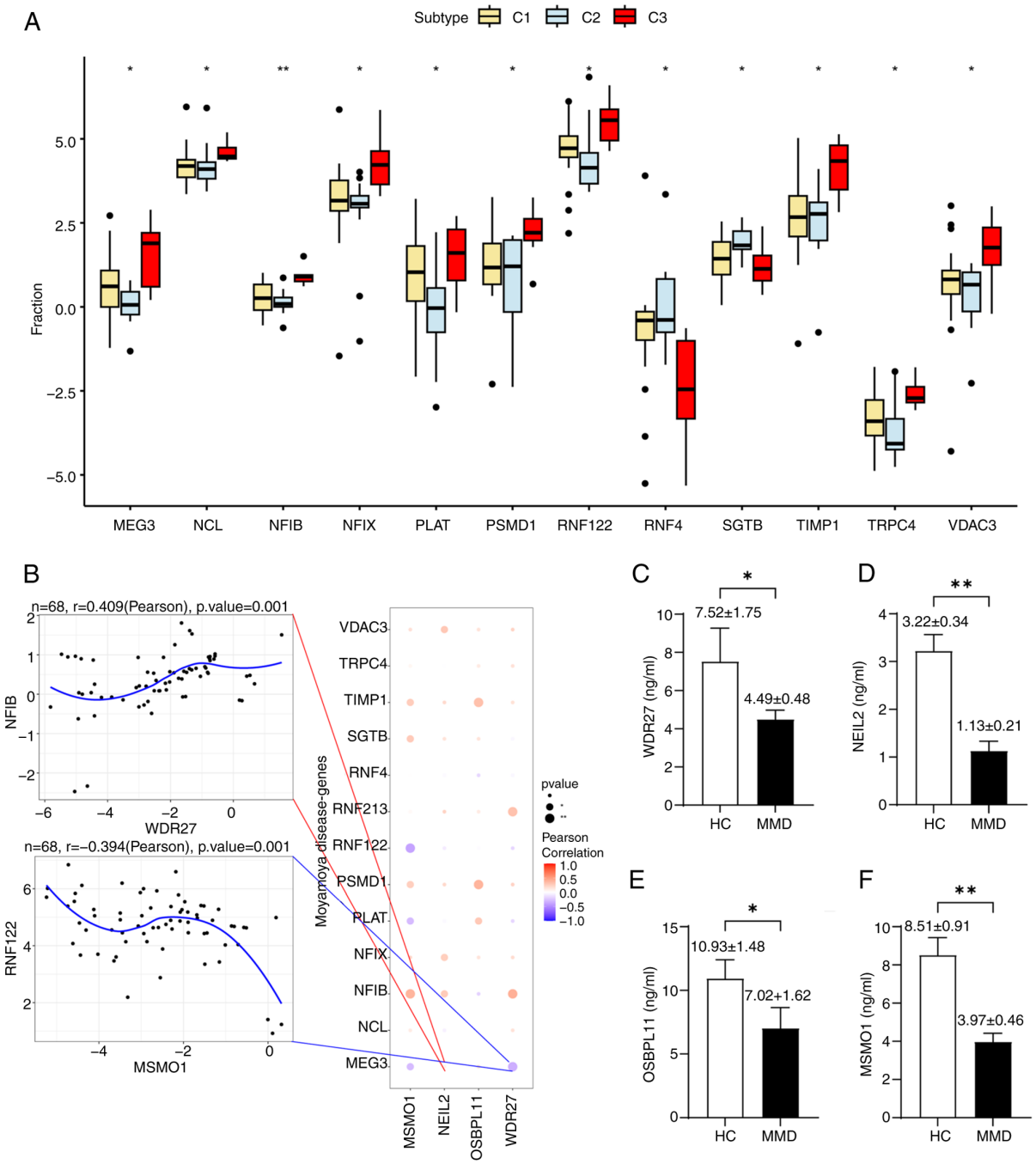

Figure 6. Relationship of hub genes and MMD-related genes and ELISA. (A) Differential analysis of MMD-related genes among different MMD molecular subgroups, including C1, C2 and C3. (B) Bubble map for the correlation between the four hub genes and MMD-related genes. The blue curves are the fitting curves of the Pearson correlation analysis. (C-F) The content of (C) *WDR27*, (D) *NEIL2*, (E) *OSBPL11* and (F) *MSMO1* was determined using ELISA kits. *P<0.05; **P<0.01. MMD, moyamoya disease; HC, healthy control.

a significant negative correlation with *GIPC1* (Pearson's r=-0.613) and *NEIL2* was significantly correlated with *SOX18* (Pearson's r=-0.575). Hub genes were also significantly related to various endothelial proliferation-related genes (Table SIV). *MSMO1* showed a significant positive correlation with *SEMA5A* (Pearson's r=0.582) and *WDR27* was significantly correlated with *MSMO1* (Pearson's r=0.737).

ELISA. The results showed that *WDR27* (P=0.045), *NEIL2* (P=0.0008), *OSBPL11* (P=0.037) and *MSMO1* (P=0.0015) were all significantly decreased in patients with MMD compared to healthy controls, as shown in Fig. 6C-F, which correlated with the results of previous bioinformatics analyses.

Discussion

The potential etiology and pathogenesis of MMD have long been studied. Reduced *RNF213* expression increases endothelial cell proliferation, migration and tube formation by inducing vascular endothelial growth factor receptor 2 overexpression (16). Takagi *et al* (17) indicated that caspase-3-dependent apoptosis occurred in the MCA media of MMD. The cell

death mechanisms may be important for exploring the potential molecular pathogenesis of MMD. Recent studies have discovered a new type of disulfide-induced cell death in human cells known as disulfidptosis. Dysregulated disulfidptosis in target cells may lead to the abnormal proliferation of endothelial cells, which could lead to chronic vascular stenosis during MMD pathogenesis. In the present study, the effects of disulfidptosis on the expression profiles of arteries occluded by MMD were explored.

The current study identified 29 significantly differentially expressed DRGs and four hub genes, namely *WDR27*, *OSBPL11*, *MSMO1* and *NEIL2*, were selected. It was hypothesized that these hub genes may be potential biomarkers for the molecular classification of MMD based on disulfidptosis. The expression levels of these four hub genes were validated using ELISA performed using serum samples from patients with MMD and healthy controls. Thereby, an additional clinical cohort was recruited to verify the differentially expressed hub genes, to validate the results obtained from the bioinformatics analyses. Disulfidptosis plays an important role in cancer and is reported to be significantly different in most cancers, such as lung adenocarcinoma and uterine corpus endometrial carcinoma, and it is also related to physiological discrepancies in different parts of the body (18). Neurological tumors are more likely to experience glucose starvation, leading to high disulfidptosis rates, affecting the response to antitumor drugs and prognosis (18). MMD, which affects the brain, may have a similar status to neurological tumors and may express abnormal levels of disulfidptosis.

A clinical trial from Japan identified the significant difference between a surgical and nonsurgical group, which suggested the preventive effect of the direct bypass against rebleeding in MMD. Furthermore, the results showed that the subgroup with perforating arteries from the choroidal artery or posterior cerebral artery had a higher risk of rebleeding, which suggested the association of hemorrhage with different vascular phenotypes in patients with MMD (19). The current study focused on the differential expression of disulfidptosis in patients with MMD and explored the effects of disulfidptosis on MMD pathogenesis. Using bioinformatic analyses of this novel cell death mechanism, a novel molecular classification of MMD was discovered, which may be validated in the future to explain the different risks in clinical MMD subgroups identified in previous studies from a molecular perspective.

Soluble CD163 and CXCL5 are reportedly increased in patients with MMD and correlated with CD163+ M2-polarized macrophages, which may be implicated in the pathogenesis of MMD (4). Wang *et al* (20) identified through proteomics that certain expressed proteins that were significantly related to the immune response may lead to increased endothelial proliferation in MMD. Therefore, in the present study, specific immune cells were chosen for the correlation analysis with hub genes by performing an immune infiltration analysis in MMD, to identify which cell types may be involved in MMD pathogenesis.

WDR27 is a scaffold protein that contains multiple WD repeats. It has been demonstrated that WDR27 is involved in the anti-tumor necrosis factor response in rheumatoid arthritis (21). Furthermore, WDR27 was also found to be related to immunity and cell movement in monkeypox infection (22). In the present study, WDR27 was also found to be significantly correlated with immune responses, such as resting CD4 memory T cells and memory B cells in MMD, which could lead to immune dysregulation related to chronic vascular stenosis. Of note, genome-wide association analyses of sleep disturbances revealed that WDR27 is related to insomnia symptoms (23).

OSBPL11 has a similar structure and sequence to OSBP, leading to similar biological functions. OSBP binds to oxysterols, which inhibit cholesterol synthesis (24). Bouchard *et al* (25) identified that OSBPL11 is related to cholesterol and glucose metabolism in obesity, which could lead to high cardiovascular disease risk. In the present study, KEGG enrichment analysis also revealed that glycan degradation pathways were significantly different between patients with MMD and controls, which may be due to abnormal glucose metabolism induced by downregulated OSBPL11 in MMD. A characteristic glucose hypometabolic pattern has been reported in patients with MMD with vascular cognitive impairment, and it has been indicated that abnormal brain glucose metabolism is related to cognitive impairment in MMD (26).

MSOM1 plays an important role in cholesterol synthesis (27). Previous studies have reported that MSMO1 promotes the development of different cancers, such as liver, breast and oligodendrogliomas (28-30). It was identified that downregulation of MSMO1 in pancreatic cancer is associated with advanced progression and poor prognosis. Epithelial-mesenchymal transition-like cell morphology and cell mobility were activated by MSMO1 knockout, indicating that MSMO1 may induce cell motility and cell migration (31). The present results also showed a similar downregulation of MSMO1 in MMD compared to controls, which may be involved in the abnormal endothelial migration in MMD.

NEIL2 is generally required to protect against oxidative DNA damage and maintain gene stability (32). A previous study has demonstrated that NEIL2-deficient mice have an increased susceptibility to inflammation with pro-inflammatory mediators (33). It has also been suggested that NEIL2 inhibits the inflammatory response in bacterial and viral infections (34). The present results also showed a significant downregulation of *NEIL2* in MMD, and *NEIL2* was significantly correlated with neutrophils, which indicated abnormal inflammation in the arterial wall that may lead to chronic occlusion in MMD. NEIL2 may have a tumor-suppressive role in various cancers, including lung adenocarcinoma, cervical cancer and breast cancer (35,36).

The current study has several limitations. First, more participants with MMD should be enrolled in studies on disulfidptosis in MMD. As the annual incidence of MMD is 0.5-1.5 per 100,000 individuals in East Asian countries but as low as 0.1 per 100,000 in other regions, including North America, the datasets retrieved with a sample size >6 yielded only four microarray datasets (2). The small sample size may increase the risk of overfitting the data and lead to bias in the results, which means that the results may not be generalized to larger populations. Second, the datasets included in the present study lacked the clinical prognosis of patients with MMD, and a prognostic model could not be constructed for different subtypes of MMD. Third, the roles of disulfidptosis in MMD were studied using

only bioinformatics analyses, which were not verified with *in vitro* experiments. The cell models could be constructed using gene knockdown/overexpression to validate the effects of differentially expressed genes in MMD. The cell viability, cell migration and ability of vascular formation could be explored between different cell groups with various cell functional assays. Bioinformatic analysis could lead to bias in the results. The connection between disulfidptosis and MMD needs to be examined in future studies. Fourth, the CIBERSORT method, a type of deconvolution algorithm, was used to perform immune infiltration analysis, which can predict the proportion of cell types that are not actually present and decrease the accuracy of the results. A high correlation may exist in the gene expression of different cell types during analysis, which might lead to unstable analysis results and decrease their accuracy.

In conclusion, in the present study, a novel molecular classification of MMD based on disulfidptosis gene expression was constructed and 348 upregulated genes and 801 downregulated genes were identified in MMD compared to controls. A total of four hub genes (*WDR27*, *OSBPL11*, *MSOM1* and *NEIL2*) were selected as biomarkers for the different subtypes of MMD. The DRG results identified that disulfidptosis may affect the progression of MMD pathogenesis. Based on this, MMD molecular subtypes were established and four hub genes were selected. Immune infiltration analysis indicated that the correlation between hub genes and immune dysfunction could lead to abnormal migration and proliferation of endothelial cells in MMD. The results of GSEA and GSVA correlated with the results of immune dysfunction. Furthermore, the expression of hub genes was validated in an internal cohort using ELISA, which was in agreement with previous analyses. To the best of our knowledge, this study was the first to explore the relationship between MMD and disulfidptosis, which may provide a new perspective to indicate a novel subtype classification of MMD and new biomarkers for the diagnosis of MMD.

Acknowledgements

Not applicable.

Funding

This research was funded by the National Natural Science Foundation of China (grant no. 82371296 to RW), which covered the expenses related to testing and processing, data collection, analysis and interpretation of the experimental data.

Availability of data and materials

The data generated in the present study may be requested from the corresponding author.

Authors' contributions

SH and RW conceived the study and designed the experiments. SH, YW, YS, JZ, ZZ and YZ collected data, performed bioinformatics analysis, performed experiments and discussed the contents. YW and YS checked and confirmed the authenticity of the raw data. All authors wrote and revised the manuscript. All authors have read and approved the final manuscript.

Ethics approval and consent to participate

This study was approved by the Institutional Ethics Committee of Beijing Tiantan Hospital (Beijing, China). The bioinformatics study was approved (approval no. KY 2023-2024-02) in 2023, while the blood samples were obtained from July 2021 to December 2022 which was approved (approval no. KY 2020-045-02) in May 2020. Written informed consent was obtained from all participants in accordance with the Declaration of Helsinki and the study protocol was approved by the Ethics Committee of Beijing Tiantan Hospital (approval no. KY 2020-045-02).

Patient consent for publication

Not applicable.

Competing interests

The authors declare that they have no competing interests.

References

1. Suzuki J and Takaku A: Cerebrovascular 'moyamoya' disease. Disease showing abnormal net-like vessels in base of brain. Arch Neurol 20: 288-299, 1969.
2. Ihara M, Yamamoto Y, Hattori Y, Liu W, Kobayashi H, Ishiyama H, Yoshimoto T, Miyawaki S, Clausen T, Bang OY, *et al*: Moyamoya disease: Diagnosis and interventions. Lancet Neurol 21: 747-758, 2022.
3. Mertens R, Graupera M, Gerhardt H, Bersano A, Tournier-Lasserve E, Mensah MA, Mundlos S and Vajkoczy P: The genetic basis of moyamoya disease. Transl Stroke Res 13: 25-45, 2022.
4. Fujimura M, Fujimura T, Kakizaki A, Sato-Maeda M, Niizuma K, Tomata Y, Aiba S and Tominaga T: Increased serum production of soluble CD163 and CXCL5 in patients with moyamoya disease: Involvement of intrinsic immune reaction in its pathogenesis. Brain Res 1679: 39-44, 2018.
5. Sun H, Li W, Xia C, Ren Y, Ma L, Xiao A, You C, Liu Y and Tian R: Angiographic and hemodynamic features in asymptomatic hemispheres of patients with moyamoya disease. Stroke 53: 210-217, 2022.
6. Takekawa Y, Umezawa T, Ueno Y, Sawada T and Kobayashi M: Pathological and immunohistochemical findings of an autopsy case of adult moyamoya disease. Neuropathology 24: 236-242, 2004.
7. He S, Zhang J, Liu Z, Wang Y, Hao X, Wang X, Zhou Z, Ye X, Zhao Y, Zhao Y and Wang R: Upregulated cytoskeletal proteins promote pathological angiogenesis in moyamoya disease. Stroke 54: 3153-3164, 2023.
8. Liu X, Nie L, Zhang Y, Yan Y, Wang C, Colic M, Olszewski K, Horbath A, Chen X, Lei G, *et al*: Actin cytoskeleton vulnerability to disulfide stress mediates disulfidptosis. Nat Cell Biol 25: 404-414, 2023.
9. Koppula P, Zhuang L and Gan B: Cystine transporter SLC7A11/xCT in cancer: Ferroptosis, nutrient dependency, and cancer therapy. Protein Cell 12: 599-620, 2021.
10. Zhang L, Rashad S, Zhou Y, Niizuma K and Tominaga T: RNF213 loss of function reshapes vascular transcriptome and spliceosome leading to disrupted angiogenesis and aggravated vascular inflammatory responses. J Cereb Blood Flow Metab 42: 2107-2122, 2022.
11. Wang M, Zhang B, Jin F, Li G, Cui C and Feng S: Exosomal MicroRNAs: Biomarkers of moyamoya disease and involvement in vascular cytoskeleton reconstruction. Heliyon 10: e32022, 2024.

12. Mamiya T, Kanamori F, Yokoyama K, Ota A, Karnan S, Uda K, Araki Y, Maesawa S, Yoshikawa K and Saito R: Long noncoding RNA profile of the intracranial artery in patients with moyamoya disease. J Neurosurg 138: 709-716, 2022.
13. Kanamori F, Yokoyama K, Ota A, Yoshikawa K, Karnan S, Maruwaka M, Shimizu K, Ota S, Uda K, Araki Y, *et al*: Transcriptome-wide analysis of intracranial artery in patients with moyamoya disease showing upregulation of immune response, and downregulation of oxidative phosphorylation and DNA repair. Neurosurg Focus 51: E3, 2021.
14. Newman AM, Liu CL, Green MR, Gentles AJ, Feng W, Xu Y, Hoang CD, Diehn M and Alizadeh AA: Robust enumeration of cell subsets from tissue expression profiles. Nat Methods 12: 453-457, 2015.
15. Fukui M: Guidelines for the diagnosis and treatment of spontaneous occlusion of the circle of Willis ('moyamoya' disease). Research committee on spontaneous occlusion of the circle of Willis (Moyamoya disease) of the ministry of health and welfare, Japan. Clin Neurol Neurosurg 99 (Suppl): 238-240, 1997.
16. Ye F, Niu X, Liang F, Dai Y, Liang J, Li J, Wu X, Zheng H, Qi T and Sheng W: RNF213 loss-of-function promotes pathological angiogenesis in moyamoya disease via the Hippo pathway. Brain 146: 4674-4689, 2023.
17. Takagi Y, Kikuta K, Sadamasa V, Nozaki K and Hashimoto N: Caspase-3-dependent apoptosis in middle cerebral arteries in patients with moyamoya disease. Neurosurgery 59: 894-900, 2006.
18. Zhao D, Meng Y, Dian Y, Zhou Q, Sun Y, Le J, Zeng F, Chen X, He Y and Deng G: Molecular landmarks of tumor disulfidptosis across cancer types to promote disulfidptosis-target therapy. Redox Biol 68: 102966, 2023.
19. Miyamoto S, Yoshimoto T, Hashimoto N, Okada Y, Tsuji I, Tominaga T, Nakagawara J and Takahashi JC: Effects of extracranial-intracranial bypass for patients with hemorrhagic moyamoya disease: Results of the Japan adult moyamoya trial. Stroke 45: 1415-1421, 2014.
20. Wang X, Han C, Jia Y, Wang J, Ge W and Duan L: Proteomic profiling of exosomes from hemorrhagic moyamoya disease and dysfunction of mitochondria in endothelial cells. Stroke 52: 3351-3361, 2021.
21. Honne K, Hallgrímsdóttir I, Wu C, Sebro R, Jewell NP, Sakurai T, Iwamoto M, Minota S and Jawaheer D: A longitudinal genome-wide association study of anti-tumor necrosis factor response among Japanese patients with rheumatoid arthritis. Arthritis Res Ther 18: 12, 2016.
22. Anuraga G, Lang J, Xuan DTM, Ta HDK, Jiang JZ, Sun Z, Dey S, Kumar S, Singh A, Kajla G, *et al*: Integrated bioinformatics approaches to investigate alterations in transcriptomic profiles of monkeypox infected human cell line model. J Infect Public Health 17: 60-69, 2024.
23. Lane JM, Liang J, Vlasac I, Anderson SG, Bechtold DA, Bowden J, Emsley R, Gill S,. Little MA, Luik AI, *et al*: Genome-wide association analyses of sleep disturbance traits identify new loci and highlight shared genetics with neuropsychiatric and metabolic traits. Nat Genet 49: 274-281, 2017.
24. Diercks AH, Podolskaia IS, Murray TA, Jahn AN, Mai D, Liu D, Amon LM, Nakagawa Y, Shimano H, Aderem A and Gold ES: Oxysterol binding protein regulates the resolution of TLR-induced cytokine production in macrophages. Proc Natl Acad Sci U S A 121: e2406492121, 2024.
25. Bouchard L, Faucher G, Tchernof A, Deshaies Y, Marceau S, Lescelleur O, Biron S, Bouchard C, Pérusse L and Vohl MC: Association of OSBPL11 gene polymorphisms with cardiovascular disease risk factors in obesity. Obesity (Silver Spring) 17: 1466-1472, 2009.
26. Weng R, Ren S, Su J, Ni W, Yang C, Gao X, Xiao W, Zhang X, Jiang H, Guan Y, *et al*: 18F-FDG PET and a classifier algorithm reveal a characteristic glucose metabolic pattern in adult patients with moyamoya disease and vascular cognitive impairment. Brain Imaging Behav 17: 185-199, 2023.
27. Kalay Yildizhan I, Gökpınar İli E, Onoufriadis A, Kocyigit P, Kesidou E, Simpson MA, McGrath JA, Kutlay NY and Kundakci N: New homozygous missense MSMO1 mutation in two siblings with SC4MOL deficiency presenting with psoriasiform dermatitis. Cytogenet Genome Res 160: 523-530, 2020.
28. Xu P, Wu M, Chen H, Xu J, Wu M, Li M, Qian F and Xu J: Bioinformatics analysis of hepatitis C virus genotype 2a-induced human hepatocellular carcinoma in Huh7 cells. Onco Targets Ther 9: 191-202, 2016.
29. Simigdala N, Gao Q, Pancholi S, Roberg-Larsen H, Zvelebil M, Ribas R, Folkerd E, Thompson A, Bhamra A, Dowsett M and Martin LA: Cholesterol biosynthesis pathway as a novel mechanism of resistance to estrogen deprivation in estrogen receptor-positive breast cancer. Breast Cancer Res 18: 58, 2016.
30. He P, Sun L, Zhu D, Zhang H, Zhang L, Guo Y, Liu S, Zhou J, Xu X and Xie P: Knock-down of endogenous bornavirus-like nucleoprotein 1 inhibits cell growth and induces apoptosis in human oligodendroglia cells. Int J Mol Sci 17: 435, 2016.
31. Cao R, Zhang Z, Tian C, Sheng W, Dong Q and Dong M: Down-regulation of MSMO1 promotes the development and progression of pancreatic cancer. J Cancer 13: 3013-3021, 2022.
32. Tapryal N, Chakraborty A, Saha K, Islam A, Pan L, Hosoki K, Sayed IM, Duran JM, Alcantara J, Castillo V, *et al*: The DNA glycosylase NEIL2 is protective during SARS-CoV-2 infection. Nat Commun 14: 8169, 2023.
33. Chakraborty A, Wakamiya M, Venkova-Canova T, Pandita RK, Aguilera-Aguirre L, Sarker AH, Singh DK, Hosoki K, Wood TG, Sharma G, *et al*: Neil2-null mice accumulate oxidized DNA bases in the transcriptionally active sequences of the genome and are susceptible to innate inflammation. J Biol Chem 290: 24636-24648, 2015.
34. Sayed IM, Sahan AZ, Venkova T, Chakraborty A, Mukhopadhyay D, Bimczok D, Beswick EJ, Reyes VE, Pinchuk I, Sahoo D, *et al*: Helicobacter pylori infection downregulates the DNA glycosylase NEIL2, resulting in increased genome damage and inflammation in gastric epithelial cells. J Biol Chem 295: 11082-11098, 2020.
35. Sarker AH, Chatterjee A, Williams M, Lin S, Havel C, Jacob P III, Boldogh I, Hazra TK, Talbot P and Hang B: NEIL2 protects against oxidative DNA damage induced by sidestream smoke in human cells. PLoS One 9: e90261, 2014.
36. Ye F, Liu J, Wang H, Chen X, Cheng Q and Chen H: Cervical carcinoma risk associate with genetic polymorphisms of NEIL2 gene in Chinese population and its significance as predictive biomarker. Sci Rep 10: 5136, 2020.